AGU PUBLICATIONS

Paleoceanography

RESEARCH ARTICLE

10.1002/2014PA002675

Key Points:
- Strong circumpolar transport does not require unblocked latitude circles
- Sensitivity to wind stress of transport changes with overlapping continents
- Changes in sensitivity to wind stress are linked to changes in momentum balance

Correspondence to:
D. R. Munday,
danday@bas.ac.uk

Citation:
Munday, D. R., H. L. Johnson, and D. P. Marshall (2015), The role of ocean gateways in the dynamics and sensitivity to wind stress of the early Antarctic Circumpolar Current, *Paleoceanography*, *30*, 284–302, doi:10.1002/2014PA002675.

Received 29 MAY 2014
Accepted 13 FEB 2015
Accepted article online 18 FEB 2015
Published online 25 MAR 2015

The role of ocean gateways in the dynamics and sensitivity to wind stress of the early Antarctic Circumpolar Current

D. R. Munday[1,2], H. L. Johnson[3], and D. P. Marshall[1]

[1] Atmospheric, Oceanic and Planetary Physics, University of Oxford, Oxford, UK, [2] British Antarctic Survey, Cambridge, UK, [3] Department of Earth Sciences, University of Oxford, Oxford, UK

Abstract The date of inception of the Antarctic Circumpolar Current is debated due to uncertainty in the relative opening times of Drake Passage and the Tasman Seaway. Using an idealized eddy-resolving numerical ocean model, we investigate whether both ocean gateways have to be open to allow for a substantial circumpolar current. We find that overlapping continental barriers do not impede a circumpolar transport in excess of 50 Sv, as long as a circumpolar path can be traced around the barriers. However, the presence of overlapping barriers does lead to an increased sensitivity of the current's volume transport to changes in wind stress. This change in sensitivity is interpreted in terms of the role of pressure drops across continental barriers and submerged bathymetry in balancing the momentum input by the surface wind stress. Specifically, when the pressure drop across continents is the main balancing sink of momentum, the zonal volume transport is sensitive to changes in wind stress. Changes in zonal volume transport take place via altering the depth-independent part of the circumpolar transport rather than that arising from thermal wind shear. In such a scenario, isopycnals continue to slope steeply across the model Southern Ocean, implying a strong connection between the deep and surface oceans. This may have consequences for the meridional overturning circulation and its sensitivity to wind stress.

1. Introduction

The Southern Ocean and Antarctic Circumpolar Current (ACC), with a zonal volume transport of 137 ± 7 Sv (1 Sv = 10^6 m^3 s^{-1}), are important to the Earth's climate in providing the major interbasin connection between the Atlantic and Indo-Pacific Ocean [*Meredith et al.*, 2011]. Indeed, it is common to describe the ACC as existing due to the belt of open latitudes that are not intersected by land within the latitude band of Drake Passage, the Southern Ocean's narrowest constriction [see, e.g., *Thompson*, 2008]. From a paleoclimate viewpoint this is troublesome, since the date at which this band of open latitudes first existed is poorly constrained. While the opening of the Tasman Seaway can be dated to sometime in the range 35.5–30 Ma, estimates of the earliest opening of Drake Passage span the range between 50 Ma and 17 Ma [*Livermore et al.*, 2005; *Barker et al.*, 2007]. Similarly, the date of the inception of the ACC also remains controversial, with estimates spanning those of the opening of Drake Passage [*Wei and Wise*, 1992; *Scher and Martin*, 2006]. The opening of these gateways may have played a significant role in the general cooling of the Cenozoic [*Sijp et al.*, 2014].

It has been assumed in the literature that the opening of Drake Passage and the Tasman Seaway are both prerequisites for a strong circumpolar current [see, e.g., *Barker et al.*, 2007; *Sijp et al.*, 2014]. However, there are good theoretical grounds to expect that only an open Drake Passage is necessary for a substantial circumpolar transport.

Recent advances in our understanding of the fluid dynamics of the ACC suggest that it can migrate northwards to a substantial degree, in order to capture wind forcing to the north of Drake Passage [*Allison et al.*, 2010]. This migration can cause the bulk of the ACC's volume transport to exist outside the band of open circumpolar latitudes at Drake Passage as seen, for example, in the eddy-permitting state estimate of *Mazloff et al.* [2010]. Modern observations [*Böning et al.*, 2008] and model simulations [*Olbers et al.*, 2007] all show large meridional excursions of the ACC to the north as it exits Drake Passage. The current then remains north of Cape Horn for much of the Indo-Pacific Basin. As a result, it is within a relatively narrow longitudinal band, between roughly 225 and 300°E that the path of the ACC is truly within the open latitude band of Drake Passage.

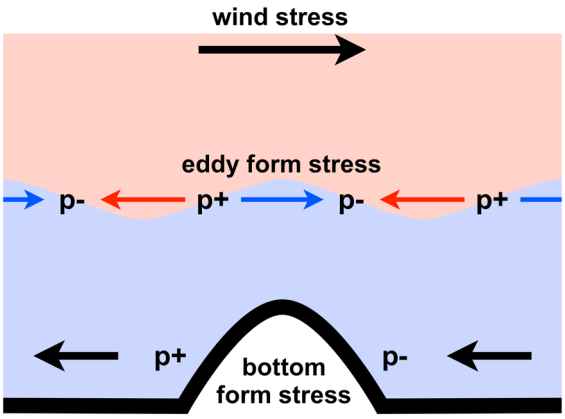

Figure 1. Schematic view of the dominant momentum balance for the modern ACC with color shading indicating different isopycnal layers in the ocean. Red shading is warm, upper layer water, and blue shading is cold, lower layer water. Black arrows indicate the direction of the stress at the surface and bottom of the ocean. Red and blue arrows indicate the stress within the isopycnal layers of the same color. The thick black line is the bottom bathymetry. The $p+$ /$p-$ indicates higher/lower than average pressure. Also, see *Vallis* [2006] and *Olbers et al.* [2012].

Within the Southern Ocean, the input of zonal momentum from the surface wind stress is balanced by bottom form stresses, i.e., a pressure difference, across the significant topography of the seabed [*Olbers*, 1998], a suggestion first made by *Munk and Palmén* [1951]. This balance is mediated by mesoscale eddies, which act to flux momentum downward [*Johnson and Bryden*, 1989] via interfacial eddy form stresses [*Ward and Hogg*, 2011]. Figure 1 illustrates the key processes that take place in this momentum balance (alternative explanations and schematics can be found in *Vallis* [2006] and *Olbers et al.* [2012]).

As shown in Figure 1, wind stress is applied at the surface and inputs momentum to the ocean, accelerating the warm, upper layer (red). This is opposed by a bottom form stress, i.e., the pressure difference across abyssal topography, which transfers the momentum to the solid Earth. The vertical transfer of momentum is provided by the eddy form stress between isopycnal layers, which is analogous to the bottom form stress, i.e., one layer pushes against the other. Where an isopycnal slopes upward, pressure is higher, and where an isopycnal slopes downward, pressure is lower. As a result, the eddy form stress decelerates the lighter, upper layer (red) and accelerates the denser, lower layer (blue). At equilibrium, the form stress at the bottom of a layer will exactly balance the form stress at the top. These concepts are key to understanding the sensitivity of zonal volume transport to wind stress in the different continental configurations of our numerical experiments.

Numerous high-resolution models indicate that the above balance between surface wind stress and bottom form stress prevails in the modern Southern Ocean [*Stevens and Ivchenko*, 1997; *Gille*, 1997; *Olbers et al.*, 2004]. The interfacial eddy form stress, required to transport momentum vertically, is equivalent to a southward eddy flux of heat/buoyancy [*Bryden*, 1979], which can be a considerable contribution to the total heat flux [e.g., *Jayne and Marotzke*, 2002; *Meijers et al.*, 2007].

Alternatively, the importance of eddies to the Southern Ocean may be viewed as being due to the requirement that the northward Ekman transport in the wind-driven surface layer be balanced by a southward return flow. In the limit that unblocked circumpolar latitudes exist, such a return flow cannot occur as a geostrophically balanced flow above the height of the bottom topography. As a result, the eddy field helps close the volume budget via its rectified "bolus" transport [*Marshall*, 1997; *Marshall and Radko*, 2003] and so play a prominent role in eliminating the so-called Deacon cell [*Danabasoglu et al.*, 1994]. The combination of the Eulerian mean flow and the opposing eddy-driven bolus transport determine the net residual circulation that transports tracers, such as temperature and carbon, in the ocean. This residual circulation can be a subtle balance between the two constituents [*Watson and Naveira Garabato*, 2006], and the eddies give rise to a much reduced sensitivity to changes in wind stress, known as "eddy compensation" [*Viebahn and Eden*, 2010; *Abernathey et al.*, 2011]. Surface temperature and salinity forcing also plays a role in setting the net residual circulation [see, e.g., *Walin*, 1982], which we do not consider in any detail.

Mesoscale eddies also play a role in the zonal circulation of the Southern Ocean. Due to their interaction with, and role in setting, the vertical stratification, they can act to limit the slope of isopycnals, and thus the zonal transport [*Straub*, 1993]. The well documented loss of sensitivity of volume transport of a circumpolar current to changes in wind stress when mesoscale eddies are resolved [*Hallberg and Gnanadesikan*, 2001; *Tansley and Marshall*, 2001] is known as "eddy saturation." It is related to the aforementioned eddy compensation, although dynamically distinct [*Meredith et al.*, 2012; *Morrison and Hogg*, 2013]. A sufficiently eddying

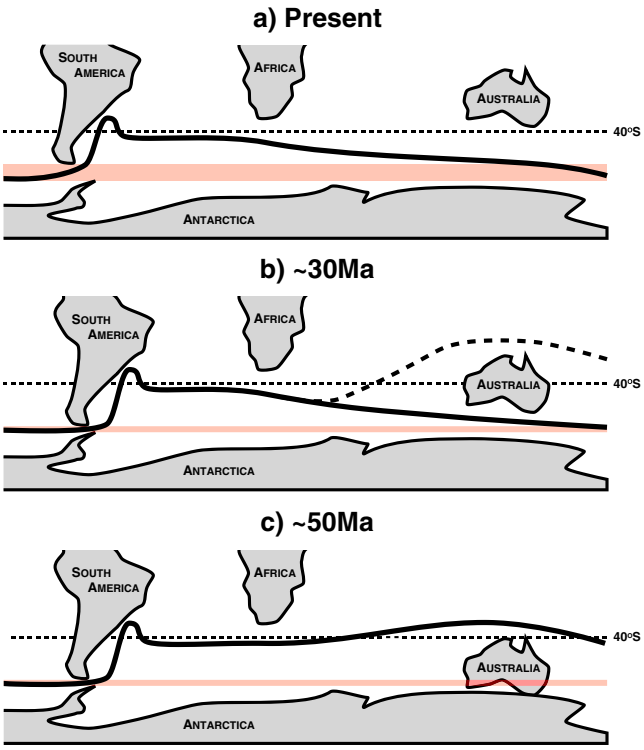

Figure 2. A schematic of the (possible) path of the Antarctic Circumpolar Current (thick black line) relative to 40°S (dashed black line) and the position of the major continents. The red-shaded region shows the latitude range of Drake Passage. (a) Modern era, ACC path based loosely on, e.g., *Mazloff et al.* [2010], (b) approximately 30 Ma with a deep, wide Tasman Seaway and narrow, shallow Drake Passage (dashed line is a potential northern route), (c) approximately 50 Ma with a closed Tasman Seaway and narrow, shallow Drake Passage. The past positions of the continents are loosely based upon the paleogeographical maps of *Blakey* [2008] and the bathymetry used by *Huber et al.* [2004] and *Sijp et al.* [2011] in their model reconstructions.

current can show zero sensitivity of its circumpolar transport to wind stress, due to increased eddy activity, even in the limit of zero wind stress [*Munday et al.*, 2013]. However, the details of this sensitivity can depend upon the specific geometry of the chosen model domain [*Hogg and Munday*, 2014]. Furthermore, surface temperature and salinity forcing play a role in setting the transport, and its sensitivity, due to changes in stratification that accompany, e.g., increased heat fluxes [*Hogg*, 2010].

Our focus here is on the zonal circulation of the Southern Ocean, i.e., the circumpolar transport and, via thermal wind shear, the global pycnocline depth and their sensitivity to wind stress changes. This is an important metric of the global ocean and its circulation, since it reflects the middepth and deep stratification throughout much of the other ocean basins [*Gnanadesikan and Hallberg*, 2000]. The processes that set the stratification are linked to those that determine the meridional overturning circulation [e.g., *Gnanadesikan*, 1999]. Therefore, understanding how changing continental geometry and ocean bathymetry may interact with the ocean's mesoscale eddy field and its role in setting ocean stratification is a good first step to understanding the wider circulation.

Given the ability of the ACC to migrate to the north of Drake Passage, it begs the question, does the inception of a circumpolar current require that both Drake Passage and the Tasman Seaway be open? Or must one merely be able to trace a circumpolar path around the continental land masses? Does the presence of surface-breaking continental barriers lead to a change in the sensitivity of the circumpolar transport to changes in wind stress? Furthermore, how might the momentum budget of a paleo-ACC differ from the well-established balance between surface wind stress and bottom form stress?

In investigating the above questions, we consider an idealized view of the plausible continental geometries shown schematically in Figure 2 for the period of time in question. In the modern world, the path of the ACC is something like that shown in Figure 2a, and as described above. In the event that Drake Passage is open prior to the Tasman Seaway, we envisage a path something like that shown in Figure 2c. In this case, the ACC is required to spend more of its path to the north of 40°S, although without being much farther north than in the modern world. This excursion may expose more of the ACC to eastward wind, based upon the winds of the modern world. However, it is the integrated wind across the full path of the ACC that is dynamically important [*Allison et al.*, 2010], and the current would remain dominantly eastward as a result of thermal wind balance. Furthermore, it seems likely that the momentum balance of surface wind stress offset by bottom form stress would remain unchanged in an eddying ocean.

Is it likely that the ACC could undergo a large enough excursion to flow over and around an Australia attached to Antarctica? In our view, yes. While the majority of model reconstructions, e.g., *Huber et al.* [2004]

and *Hill et al.* [2013], do not show the ACC doing so, there is certainly a precedent in the modern world for large changes in latitude (see above). Furthermore, the recent model simulations of *Sijp et al.* [2011] show strong circumpolar transport around an attached Australia (their Figure 5a). In addition, when the Tasman Seaway is unblocked in their model, the ACC follows both a northern route and a southern route around the land mass (their Figure 5b), shown schematically in Figure 2b.

If an ACC were to exist in the scenario illustrated in Figure 2c, then it would have to flow through a narrow Drake Passage and around a large landmass (Australia) in order to complete its circumpolar path. This configuration is rather different to modern geography. In particular, the absence of any open latitudes in Drake Passage (the red shading in Figure 2c) is reminiscent of the work of, for example, *Webb* [1993] on the path and nature of circumpolar currents when obstructions to the flow are present.

In the model of *Webb* [1993], the addition of barriers blocking "Drake Passage" changes the character of the circumpolar current's path. The solid walls act as boundaries to support frictional western boundary currents balanced by the pressure change across the basin. As a result, the circumpolar current breaks down into a series of quasi-zonal currents linked by western boundary currents. The formation of these piecewise zonal currents is a familiar aspect of other linear models of the ACC (see *LaCasce and Isachsen* [2010] for a review). In such models, the Southern Ocean is represented as an idealized (barotropic) channel with bottom friction playing a major role in the dynamics due to the strong bottom flow when the bottom is flat. The zonal transport of such models is typically very high. However, the development of an equivalent barotropic model by *Krupitsky et al.* [1996], in which fixed vertical stratification results in the thermal wind shear being in the direction of the flow at a given reference level, can give more realistic transport values.

Given the uncertainty regarding continental geometry and surface forcing, we choose to investigate the above questions using an idealized configuration of the Massachusetts Institute of Technology general circulation model (MITgcm). Our aim is to investigate the relevance of theoretical ideas based on the modern ACC to its inception and early history. Specifically, to investigate the role of eddy saturation, and the momentum balance between wind stress and bottom form stress, under changing continental geometry. To do so, we adopt an idealized model designed to address the questions proposed above in a baroclinic model with a vigorous mesoscale eddy field.

In section 2 we describe the details of the model configuration. In section 3 we discuss the results obtained from a range of bathymetric configurations, paying particular attention to the circumpolar transport and its sensitivity to wind stress. In section 4, we analyse the momentum budget and connect its variation to the changes in circumpolar transport discussed in section 3. Finally, we close with a summary of our conclusions and discussion of our results in section 5.

2. Model Numerics and Domains

In order to investigate the effects of continental obstructions on the eddy saturation and momentum budget of a circumpolar current, we employ the MITgcm [*Marshall et al.*, 1997a, 1997b] in an idealized eddy-resolving channel configuration. This allows many experiments under different combinations of forcing and bathymetry to be conducted. Geometrically, the model domain takes the form of a zonal channel shown schematically in Figure 3. Such models have a singular provenance with regard to our understanding of the physics of the Southern Ocean, see, for example, *Abernathey et al.* [2011, and references therein].

The domain used here is a total of 9600 km long and 2000 km wide. All of the presented experiments use a maximum depth of 3000 m, although some include a 1500 m high submerged bathymetric ridge and/or continental barriers. In the vertical, the model domain has 30 unevenly spaced levels. The surface layer is the thinnest, at 10 m, while the bottom five levels have a common thickness of 250 m. The model uses a Cartesian grid on a β plane with a uniform horizontal grid spacing of 10 km (the deformation radius is approximately 18 km in the centre of the channel and the eddies that are generated are typically several multiples of the deformation radius in size; see Figure 4d) and an implicit linear free surface. The specifics of the numerical methods are important to the fidelity of the eddy field and the simulation of circumpolar current dynamics. More details are given in the appendix.

In terms of the geometry of the Eocene ocean/landmasses, and the schematic of Figure 2, a continental barrier on the channel's southern boundary represents Australia as still connected to Antarctica. A continental barrier extending from the northern boundary is an idealized South America and forms the

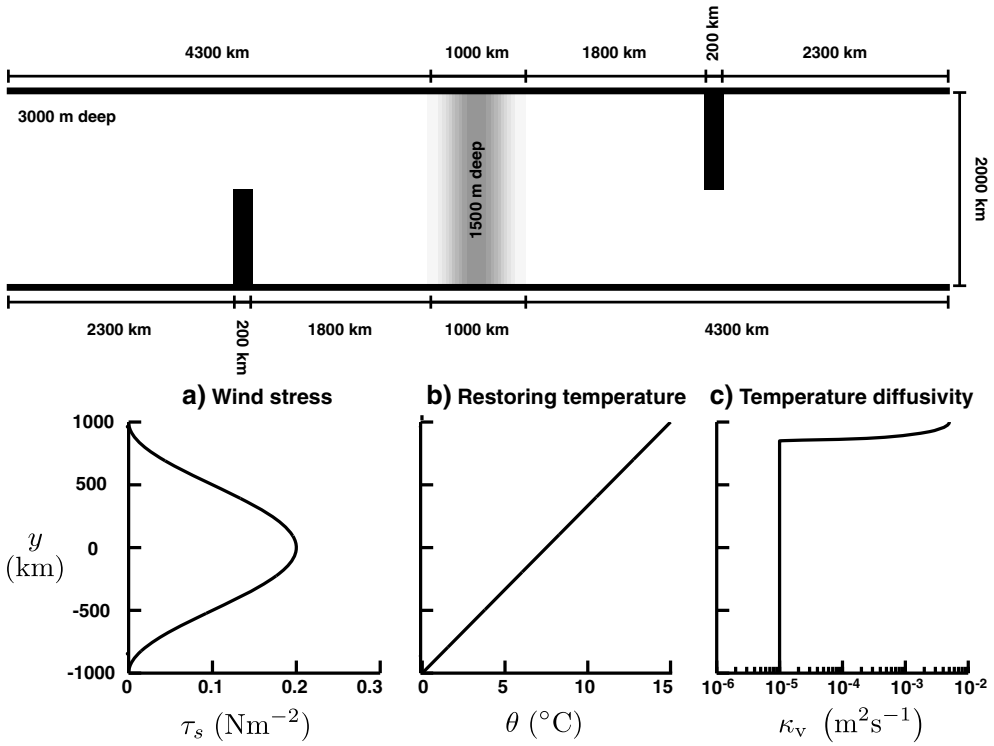

Figure 3. Schematic of the eddy-resolving MITgcm channel model of the Southern Ocean. The solid black lines are the northern and southern boundaries of the channel, and the black rectangles mark the position of the full depth continental barriers. The channel is 3000 m deep, except over the ridge (the grey-shaded area), where it is 1500 m deep. (a) Surface wind stress, (b) surface restoring temperature, and (c) vertical temperature diffusivity.

model's Drake Passage. We have not included a version of the Antarctic Peninsula. In order to simplify the model geometry and set up, the bathymetry of the Southern Ocean has been collected together in a single ridge at the midpoint of the channel. This represents, for example, the combined ridge that would be expected in Drake Passage and the Tasman Seaway. Collecting the bottom bathymetry in this way makes the decomposition of the pressure gradient into bottom and continental form stress (see section 4.1) terms considerably cleaner. The main purpose of the ridge is to allow for a pressure gradient across its width, which can then balance the surface wind stress, as in the momentum budget discussed in section 1. A single bathymetric obstacle is sufficient for this purpose [see, e.g., *Tansley and Marshall*, 2001].

In the spirit of the idealized geometry, we choose similarly idealized surface forcing and boundary conditions. Wind forcing is applied as an idealized zonal jet with the peak wind stress in the center of the channel. The shape of this jet is given by

$$\tau_s = \frac{\tau_0}{2}\left(1 + \cos\left(\frac{2\pi y}{L_y}\right)\right), \tag{1}$$

where L_y is the meridional width of the channel and is shown graphically in Figure 3a for the control wind forcing of $\tau_0 = 0.2$ N m^{-2}. No meridional wind stress is applied. The chosen control wind stress is typical of that used in other idealized model studies, e.g., *Abernathey et al.* [2011] or *Munday et al.* [2013], and of the climatological wind stresses obtained in coupled climate models, e.g., *Russell et al.* [2006] or *Meijers et al.* [2011]. Other values of τ_0 are used in a series of perturbation experiments as described below.

For potential temperature, we choose a simple restoring condition with an idealized meridional profile. The functional form of the surface restoring temperature is given by

$$\theta = \left(\frac{y + L_y/2}{L_y}\right)\Delta\theta \tag{2}$$

where $\Delta\theta$ is the temperature difference between the southern and northern boundary regions. This temperature restoring condition is illustrated graphically in Figure 3b and all of the experiments used here use $\Delta\theta = 15$ K.

Low-latitude and northern high-latitude processes, such as deep water formation or diapycnal diffusivity, can act to alter the global pycnocline depth [*Gnanadesikan*, 1999] and impact the transport of circumpolar currents [*Munday et al.*, 2011]. For this reason, we employ an enhanced vertical diffusion within 150 km of the northern boundary, as shown in Figure 3c. This enhanced diffusivity increases sinusoidally towards the northern boundary and acts to deepen the stratification and energize the eddy field, as per *Hogg* [2010]. The maximum vertical diffusivity is 5×10^{-3} m^2 s^{-1} and is roughly equivalent to a diffusivity of 1×10^{-5} m^2 s^{-1} (the value used elsewhere in the channel) operating over the global ocean area to the north of the Southern Ocean. Other standard model parameters are as given in Table 1.

3. Experimental Results

This section presents the results of 40 eddy-resolving channel models using a combination of four different continental geometries with/without a submerged bathymetric ridge and five different wind stresses. The standard eight experiments, which use the wind stress given by $\tau_0 = 0.2$ N m^{-2} (Figure 3a), include no continental barriers (FLATB and RIDGE), a single continental barrier extending from the northern boundary to the midpoint of the channel (SOLOB and RSOLO), a pair of continental barriers extending from either boundary that meet in the middle (DOUBL and RDOUB), and a pair of continental barriers that overlap by 500 km (OVERL and ROVER). These experiments are summarized in Table 2 and are run for a total of 620 model years, at which point the domain-averaged temperature is varying by < 0.01°C/century. A 20 year diagnostic window, from which all averages presented below are drawn, is then performed and a number of wind stress perturbation experiments begun. These perturbation experiments use τ_0 of 0.0, 0.1, 0.3, and 0.4 N m^{-2}. They are begun from the end of model year 620 of the standard eight experiments and run for 180 model years, at the end of which a 20 year diagnostic run is again performed.

3.1. Experimental Overview

Regardless of the details of the bottom bathymetry and/or continental configuration, the combination of surface wind stress and steeply sloping isotherms drives a strong circumpolar transport through the channel. With a flat bottom, the circumpolar transport is in excess of 650 Sv and the mean flow has little along-channel variation. As shown in Figure 4a, the Eddy Kinetic Energy (EKE) is distributed uniformly along the channel and contours of depth-integrated stream function are almost zonal.

The introduction of a submerged bathymetric ridge in experiment RIDGE has a number of effects. First, the blocking of f/H contours (where f is the Coriolis frequency and H is the ocean depth) is expected to steer circumpolar currents due to conservation of potential vorticity [*Marshall*, 1995], which acts to direct the flow along rather than across lines of constant f/H. As a result, the depth-integrated stream function shows closed gyre circulations, instead of purely zonal streamlines. Second, the EKE is now concentrated downstream of the ridge in the standing wave pattern that is characteristic of such channel flow. Third, the pycnocline depth is much shallower, as is typical of such experiments. As shown in Table 2, the domain average EKE drops from the FLATB value of 84.1 cm^2 s^{-2} to 52.0 cm^2 s^{-2} upon the introduction of a submerged bathymetric ridge, although the localization behind the bathymetric ridge leads to higher extreme values.

Including overlapping continental barriers further modifies the mean flow and its variability as shown in Figure 4c for the ROVER experiment. There is a further drop in domain average EKE of around 25% (between RIDGE and ROVER) and the occurrence of standing waves downstream of the continental barriers also leads to concentration of EKE in these locations. A similar phenomenon occurs without the submerged bathymetric ridge, i.e., even with a flat bottom the continents concentrate the EKE spatially. The inclusion of continental barriers also leads to the generation of depth-integrated wind-driven gyres and western boundary currents. These occur in all six of the control experiments that include one or more continental barriers. In the case of those that also include a bathymetric ridge, this leads to subdivision of the gyres that form due to the blocked f/H contours (cf. Figures 4b and 4c). A representative example of the instantaneous relative vorticity field corresponding to the mean flow of ROVER is shown in Figure 4d. This demonstrates the vigor of the eddy field, as well as the variation in size and intensity of the eddies throughout the channel.

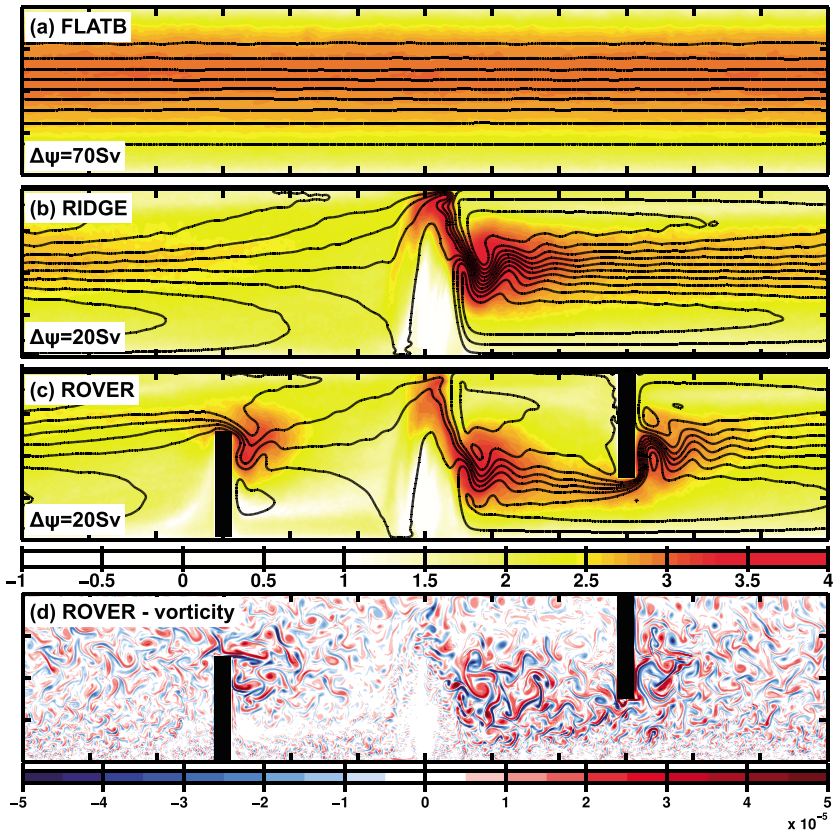

Figure 4. (a–c) The 20 year averaged mean flow after 620 model years using the control wind stress of $\tau_0 = 0.2$ N m^{-2}. Colors are EKE on a logarithmic color scale in units of cm^2 s^{-2}, and black contours are depth-integrated transport stream function with the contour interval specified in the bottom left-hand corner of each panel. Flat bottom in Figure 4a including bathymetric ridge centred in the middle of the domain in Figure 4b, and bathymetric ridge and two overlapping continental barriers (solid black) in Figure 4c. (d) The instantaneous relative vorticity field for the mean flow in Figure 4c with the colors as shown beneath.

The change in character of the currents is reminiscent of the theoretical model of *Webb* [1993] and other linear models of the ACC [*LaCasce and Isachsen*, 2010] discussed in section 1. The currents in our model results have been significantly modified from the barotropic model of *Webb* [1993] by the inclusion of a vigorous mesoscale eddy field and the baroclinic nature of the stratification. Nevertheless, the pattern of the flow that emerges could still be described in terms of regions of high/low pressure to either side of the continents and the geostrophic flow that would emerge.

3.2. Circumpolar Volume Transport

The circumpolar transport varies quite substantially as submerged bathymetry and continental topography are added to the model domain and wind stress is varied. The addition of the submerged bathymetric ridge leads to an order of magnitude reduction in the "barotropic" transport by closing the f/H contours. This reduces the flow within the bottom level, and every other model level, and allows the transport to be dominated by that arising from thermal wind shear. To illustrate this, we decompose the total transport into components due to the bottom flow and the "thermal wind." The total flow is given by

$$T_{ACC} = \int_{-H}^{0} \int_{-L_y/2}^{L_y/2} \widehat{\overline{u}}\, \mathrm{d}y\, \mathrm{d}z, \tag{3}$$

where the angled hat represents a zonal average and the overbar a time average. The "bottom flow" component is given by

$$T_b = H \int_{-L_y/2}^{L_y/2} \widehat{\overline{u}}_b\, \mathrm{d}y, \tag{4}$$

Table 1. Standard Model Parameters

Parameter	Symbol	Value	Units
(Bi) harmonic Leith coefficients (momentum)	L_ν	2.0	–
Biharmonic diffusivity (θ)	κ_4	10^9	m^4/s
Bottom drag coefficient	r_b	1.1×10^{-3}	m/s
Coriolis parameter	f_0	-1.11×10^{-4}	km
Domain size	L_x, L_y	9600, 2000	km
Domain depth	H	3000	m
Gradient in Coriolis parameter	β	1.47×10^{-11}	$m^{-1}\ s^{-1}$
Grid spacing	Δ	10	km
Reference density	ρ_0	1035	kg/m^3
Restoring time scale (θ)	t_θ	10	days
Thermal expansion coefficient	α	2×10^{-4}	K^{-1}
Vertical diffusivity (θ)	κ_v	10^{-5}	m^2/s
Vertical viscosity (momentum)	ν_v	10^{-4}	m^2/s
Wind stress magnitude	τ_0	0.2	N/m^2

where the b subscript indicates the flow in the bottom model level and H is the total depth of the water column. This quantity is the bottom flow integrated through the full depth of the water column. The thermal wind flow is then the difference, i.e.,

$$T_{\mathrm{tw}} = \int_{-H}^{0} \int_{-L_y/2}^{L_y/2} \left(\widehat{\widehat{u}} - \widehat{\widehat{u}}_b \right) \mathrm{d}y\, \mathrm{d}z = T_{\mathrm{ACC}} - T_b. \tag{5}$$

T_{tw} has a close relationship with the pycnocline depth [see, e.g., *Gnanadesikan and Hallberg*, 2000; *Munday et al.*, 2011], with their magnitudes covarying as shown in Table 2. This indicates that this is a meaningful decomposition in terms of the influence of thermal wind shear on the transport.

Table 2 and Figure 5 both indicate that with a flat bottom and no continental topography, the total transport of the circumpolar current is roughly 4 times that observed for the ACC. This is a manifestation of "Hidaka's dilemma," in which a flat-bottomed model with realistic friction parameters produces an exaggerated zonal transport [*Hidaka and Tsuchiya*, 1953] and requires excessively large frictional parameters to produce a realistic circumpolar transport [*Gill and Bryan*, 1971] (see section 4.1 for details in terms of the zonal and depth integrated momentum budget). In the case of FLATB, this leads to 80% of its total transport residing in T_b.

There is a dramatic drop in the total transport between FLATB and RIDGE due to the bathymetric ridge closing all of the f/H contours, such that the bottom flow is reduced by a factor in excess of 20 (note the change in the magnitude of the ordinate between Figure 5a and Figure 5b). In contrast to FLATB, RIDGE has ~75% of its total circumpolar transport due to the effects of thermal wind shear despite its relatively shallow pycnocline.

Table 2. Experimental Suite and for the Control Experiments, Domain Average EKE, Total Circumpolar Transport (T_{ACC}), Bottom Flow Component (T_b), Thermal Wind Component (T_{tw}), Percentage Breakdown of Transport, and Pycnocline Depth (as Defined by *Gnanadesikan* [1999])

Experiment	Ridge	North Barrier	South Barrier	Overlap?	EKE ($cm^2\ s^{-2}$)	T_{ACC} (Sv)	T_b (Sv)	T_{tw} (Sv)	% T_b/T_{tw}	z_θ (m)
FLATB	N	N	N	-	84.1	655	525	131	80/20	1222
SOLOB	N	Y	N	-	62.5	395	310	85	78/22	1112
DOUBL	N	Y	Y	N	55.8	222	155	67	70/30	1033
OVERL	N	Y	Y	Y	39.8	93	47	47	50/50	925
RIDGE	Y	N	N	-	52.0	94	24	71	25/75	990
RSOLO	Y	Y	N	-	44.7	84	26	58	30/70	937
RDOUB	Y	Y	Y	N	44.9	81	25	56	30/70	916
ROVER	Y	Y	Y	Y	41.2	68	20	48	30/70	893

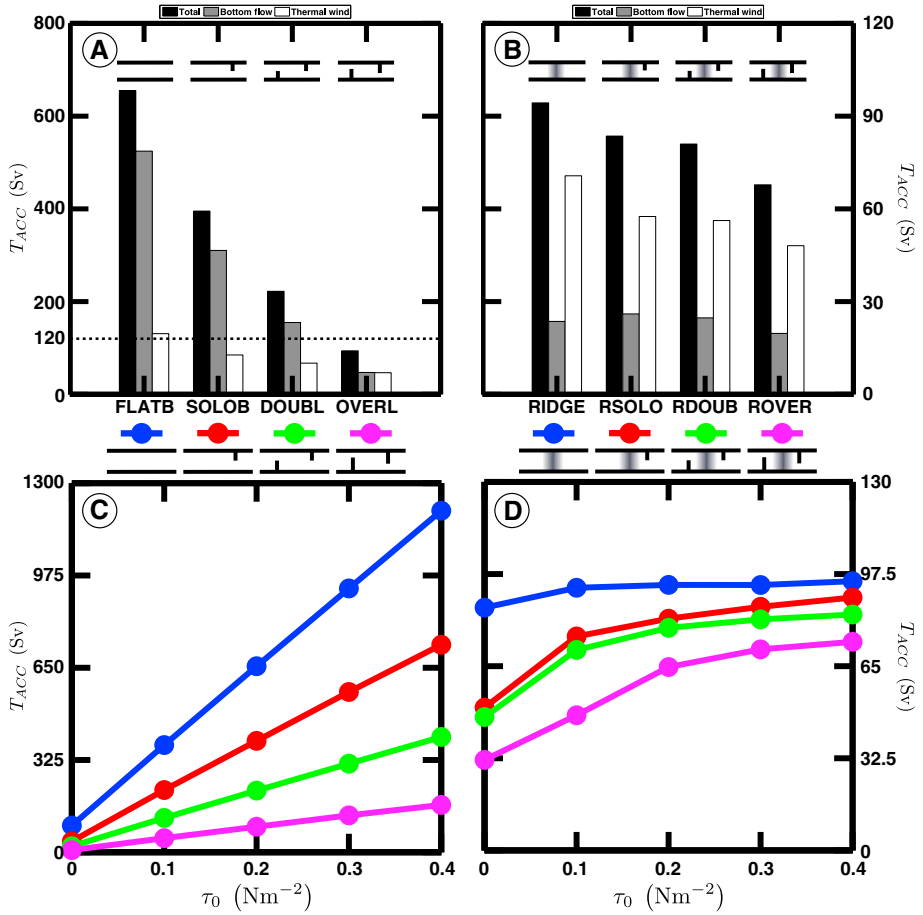

Figure 5. (a) Circumpolar transport (T_{ACC}) for control experiments with a flat bottom, including breakdown into T_b and T_{tw}, (b) as Figure 5a for experiments with a bathymetric ridge, (c) sensitivity to wind stress of T_{ACC} for flat bottomed experiments, and (d) sensitivity to wind stress of T_{ACC} for ridged experiments. The small glyphs schematically indicate the geometry under consideration in each panel.

The introduction of continental topography leads to changes in both T_b and T_{tw} for experiments with and without a bathymetric ridge. With a flat bottom, the addition of continents gives a systematic drop in T_b. The introduction of standing waves also fluxes more heat southward in time mean currents, reducing the pycnocline depth and thus T_{tw}, due to the increased efficiency of heat transport when standing waves are present [*Abernathey and Cessi*, 2014]. When the continents are overlapping in OVERL, T_b and T_{tw} are equal in magnitude, since T_b drops proportionately faster. In contrast, with a bathymetric ridge, both components of the total transport decrease at the same rate as continents are added such that the ratio T_b:T_{tw} is approximately constant. The details of the decomposition into T_b and T_{tw} can affect the quantitative details discussed here. However, the broad strokes hold for other choices, such as calculating T_b and T_{tw} at a specific longitude instead of using zonal-averaged velocity.

For our experiments including a bathymetric ridge (and also the OVERL experiment), the circumpolar transport is comparable to that attained by the coupled climate model of *Hill et al.* [2013] when their model's Drake Passage is open. Their coupled model includes complicated bathymetry and forcing, although it does not resolve mesoscale eddies. Furthermore, all five of their geometries have an open Tasman Seaway, and so there is always an open band of latitudes passing through Drake Passage.

It is clear from the results in Figure 5 that the presence of overlapping continental barriers is no impediment to a significant circumpolar transport. As such, it seems plausible that a proto-ACC could have existed prior to the opening of the Tasman Seaway, provided that Drake Passage was already open and sufficiently deep. However, what constitutes "open and sufficiently deep" remains an unresolved question (see section 5 for a discussion). The circumpolar transport attained would have then depended upon the details of

continental and bathymetric geometry, as well as the surface boundary conditions, global diapycnal mixing, etc. Even if existing proxy measurements are insufficient to determine the exact transport of any proto-ACC prior to the opening of Drake Passage, the probable presence of a circumpolar current implies the sloping of isopycnals across the Southern Ocean. Such sloped isopycnals then allow the inference of a connection between the surface waters at high southern latitudes and the deep water that may originate to the north. In turn, this suggests that the changes in the zonal circulation would have been accompanied by changes in the meridional overturning, and thus the transport of tracers such as heat and carbon, as the continental configuration changed through time.

3.3. Sensitivity to Wind Stress of Circumpolar Transport

Increasing or decreasing τ_0 leads to changes in the total circumpolar transport that are sensitive to the presence of submerged bathymetry and continental topography. The variation of the total transport with τ_0 varying from 0 to 0.4 N m^{-2} is shown in Figures 5c and 5d, for experiments with and without submerged bathymetry, respectively.

For the flat-bottomed experiments in Figure 5c, the circumpolar transport is linearly dependent upon peak wind stress, irrespective of the presence of continental topography. A finite circumpolar transport is maintained even at $\tau_0 = 0$ N m^{-2}, due to the thermal wind response to the steep across-channel slope of the isopycnals. In the FLATB geometry experiments, T_b is effectively zero at zero wind and all of the circumpolar transport is due to T_{tw}. For the case of the experiments with two overlapping continental ridges (magenta line), the net transport is very close to zero, since T_b and T_{tw} almost exactly offset each other. This is due to T_{tw} pushing eastward against the continents and the opposing push of the continents accelerating the flow westward in the bottom layers. However, undue significance should not be placed upon this, since the decomposition into T_b and T_{tw} is sensitive to whether one uses zonal averages or evaluates the transport at a particular location in the channel.

The addition of the bathymetric ridge in Figure 5d leads to a different picture (note the order of magnitude difference in the ordinate between Figure 5c and Figure 5d). With no continental topography (blue line), an eddy-saturated current results, in which the total mean transport is effectively invariant under changing wind forcing. However, the presence of one or more continental obstacles results in the reintroduction of sensitivity at low winds, typically when $\tau_0 < 0.2$ N m^{-2}, i.e., below modern climatological mean values. This is particularly noticeable for the set of experiments with ROVER bathymetry/continents (the magenta line in Figure 5d).

4. The Momentum Budget of the ACC

In this section the vertically and zonally integrated momentum budget will be used to investigate the dynamics behind the reintroduction of sensitivity to wind stress of the circumpolar transport by the placement of continental barriers. In section 4.1 we present the derivation of this budget in the interests of clarity. In section 4.2, we apply the budget to our model results. These sections help us to understand, and provide supporting evidence for, our main conclusions, i.e., that an open Tasman Seaway is not essential to a strong circumpolar transport and that the presence of overlapping continents reintroduces sensitivity to wind stress of this transport. However, a full understanding of these extra results is not strictly necessary.

4.1. Derivation of the Momentum Budget for Circumpolar Currents

Neglecting viscous terms, the zonal component of the vector invariant momentum equations is given by

$$\frac{\partial u}{\partial t} - \left(f + \xi\right) v + w\frac{\partial u}{\partial z} = -\frac{\partial B}{\partial x} + \frac{1}{\rho_0}\frac{\partial \tau_x}{\partial z}, \tag{6}$$

where $\mathbf{u} = (u, v, w)$ is the three-dimensional velocity vector and $\xi = \mathbf{k} \cdot \nabla \times \mathbf{u}$ is the vertical component of the relative vorticity. In the vector-invariant momentum equations, a vector calculus identity is applied to the nonlinear advection of momentum such that $(\mathbf{u} \cdot \nabla)\mathbf{u}$ is written as $\xi \mathbf{k} \times \mathbf{u} + \nabla(\mathbf{u} \cdot \mathbf{u}) + w\partial \mathbf{u}/\partial z$. In addition, $B = p/\rho_0 + \mathbf{u} \cdot \mathbf{u}/2$ is the Bernoulli potential, broadly equivalent to pressure itself, and τ_x is the zonal component of the total stress, i.e., wind stress, etc., acting on the fluid.

Equation (6) is integrated in the vertical, from the bottom of the domain to $z = 0$. After taking a long-term time average at steady state and applying Reynolds averaging, i.e., $u = \overline{u} + u'$, it becomes

$$-f\left[\overline{v}\right] - \left[\overline{\xi v}\right] + \left[\overline{w\frac{\partial u}{\partial z}}\right] = -\left[\frac{\partial \overline{B}}{\partial x}\right] + \frac{\tau_s}{\rho_0} - r_b \overline{u}_b, \tag{7}$$

where overbars and primes indicate time-averaged quantities and time-varying perturbations, respectively, and square braces indicate the vertical integral, i.e., $[\phi] = \int_{-H}^{0} \phi \, dz$. In addition, the gradient of EKE has been combined with the Bernoulli potential, such that $\overline{B} = p/\rho_0 + \left(\overline{u}^2 + \overline{v}^2\right)/2 + \left(\overline{u'u'} + \overline{v'v'}\right)/2$. Consistent with the formulation of the numerical model, the surface stress has been expressed as a wind stress, τ_s/ρ_0, and the bottom stress as linear friction acting on the bottom velocity, u_b, with a coefficient of r_b.

Due to the linear free surface the vertical velocity at $z = 0$ is not zero, although $w \ll (u, v)$. Once vertically integrated the term resulting from the vertical advection of horizontal momentum is several orders of magnitude smaller than the remaining terms. These terms are henceforth neglected, although they are retained in the model diagnostics for completeness.

Equation (7) is integrated zonally, from one end of the channel to the other, to give

$$0 = \int_0^{L_x} \overline{B}_{-H} \frac{\partial H}{\partial x} \, dx - \int_0^{L_x} \frac{\partial}{\partial x}\left[\overline{B}\right] dx + \frac{\langle \tau_s \rangle}{\rho_0} - r_b \left\langle \overline{u}_b \right\rangle + \left\langle \overline{\xi v} \right\rangle. \tag{8}$$

In equation (8), the Bernoulli term has been integrated by parts in the vertical and angled braces indicate the combination of vertical and zonal integration. In addition, the nonlinear vortex force, $\left\langle \overline{\xi v} \right\rangle$, has been moved to the right-hand side for clarity. At steady state, when the free surface is no longer adjusting, the continuity equation indicates that the vertical and zonal integral of the meridional velocity, $\left\langle \overline{v} \right\rangle$, is zero. As a result, there is no Coriolis term in equation (8).

The first term of equation (8) is the bottom form stress due to differences in the Bernoulli potential across submerged bathymetry at the bottom of the water column. The second term is due to Bernoulli potential changes across surface-breaking continental topography and could be transformed into a form stress (the product of the Bernoulli potential with the gradient in width) with a change of coordinates such that the variable width of the channel was taken into account. The third term is the input of zonal momentum due to the surface wind stress, and the fourth is the sink due to linear bottom friction and the no-slip bottom boundary condition. The final term is a combination of Reynolds stresses and mean flow advection, and in general is expected to be small.

When there is neither submerged bathymetry nor surface-breaking continental topography, the budget expressed in equation (8) can be further simplified to

$$\frac{\langle \tau_s \rangle}{\rho_0} - r_b \left\langle \overline{u}_b \right\rangle + \left\langle \overline{\xi v} \right\rangle = 0. \tag{9}$$

In the limit of no nonlinear advection of momentum, this expresses the well-known balance of surface wind stress balanced by bottom friction such that the bottom flow will accelerate until this balance is achieved [see, e.g., *Gill and Bryan*, 1971; *Bryan and Cox*, 1972]. The physics of this balance leads to the aforementioned Hidaka's dilemma [*Hidaka and Tsuchiya*, 1953], in which a realistic transport can only be obtained with excessive frictional coefficients. This result is illustrated in Figure 6a, using the results of experiment FLATB, which also demonstrates that the remaining terms in the budget are small, even though a finite viscosity is used for numerical reasons.

For a circumpolar current with significant bottom topography, the expected momentum balance is somewhat different. In this case, the bottom form stress is no longer zero, although the continental form stress is, and the blocking of f/H contours enforces $u_b \approx 0$. In other words, the momentum balance is more closely given by

$$\frac{\langle \tau_s \rangle}{\rho_0} + \int_0^{L_x} \overline{B}_{-H} \frac{\partial H}{\partial x} \, dx + \left\langle \overline{\xi v} \right\rangle = 0. \tag{10}$$

The eastward momentum input by the wind is now balanced by the bottom form stress, transmitted vertically through the water column via interfacial eddy form stresses as per Figure 1. As with the flat-bottomed

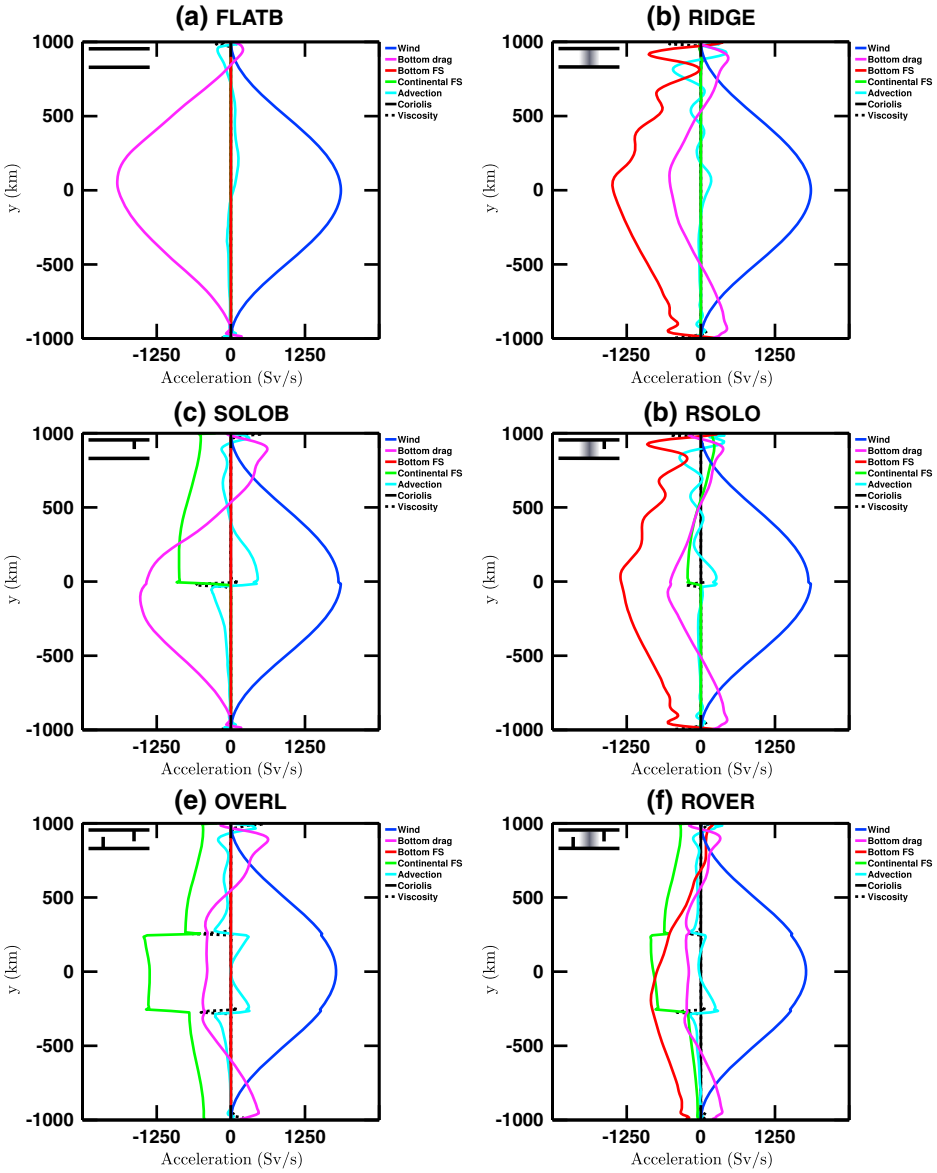

Figure 6. The 20 year time-average vertically and zonally integrated zonal momentum budget after 620 model years. The terms are as described in equation (8), i.e., wind stress (blue), bottom drag (magenta), bottom form stress (red), continental form stress (green), and nonlinear advection/Reynolds stress (cyan), with the addition of the Coriolis term (solid black) and viscous terms (dashed black), which are both small. The small glyphs schematically indicate the geometry under consideration in each panel.

momentum balance, this is also a well-known result [see, e.g., *Stevens and Ivchenko*, 1997; *Jackson et al.*, 2006]. It is illustrated in Figure 6b using the results of experiment RIDGE. The increased magnitude and changing sign of the vortex force, $\left\langle \overline{\xi}\overline{v} \right\rangle$, is due to the presence of standing waves across the submerged bathymetry, which leads to increased Reynolds' stresses on the flow. Due to the blocked f/H contours generating barotropic gyres, the bottom friction term takes on an oscillatory character that is negative near the boundaries and positive in the center. This reflects the structure of the barotropic gyres, which are westward near the boundaries and eastward in the center, seen in Figure 4b.

When continents are added to the model domain, it is no longer obvious that the remaining terms are small. In particular, the presence of full-depth barriers to the flow mean that the continental form stress may now be nonzero. This could potentially modify the simple balances presented in equations (9) and (10) and may explain the differing sensitivities seen in Figures 5c and 5d.

4.2. Momentum Budget With Continental Ridges

In experiment SOLOB a single continental ridge is added to the northern boundary, leading to a distinct change in character of the momentum budget. As shown in Figure 6c, the model retains the prevalent balance of FLATB in the southern half of the domain. However, in the northern half of the domain, the sink of momentum due to bottom friction takes on the character of the barotropic gyre that forms due to the presence of a solid western boundary. In this half of the domain a three-way balance between surface wind stress, bottom friction, and continental form stress now exists. Note that because the mean current close to the northern boundary is westward, the eastward linear bottom friction is still acting as a sink of momentum.

When the model domain includes a submerged bathymetric ridge, the change in the momentum balance from the inclusion of a continental ridge on the northern boundary is not as profound. The continental form stress in the momentum budget of experiment RSOLO, see Figure 6d, is of approximately the same magnitude as the nonlinear Reynolds stresses and bottom friction. As such, the dominant balance in the channel retains the character of the RIDGE experiment with the mesoscale eddy field successfully transmitting the momentum input of the wind vertically in order to balance it with bottom form stress.

Experiments OVERL and ROVER include a pair of continental barriers that overlap by 500 km. This causes changes in the momentum balance of both experiments, with respect to SOLOB and RSOLO, as shown in Figures 6e and 6f. In particular, continental form stress can now play a role across the full meridional extent of the channel rather than in just one half of the domain. In both experiments the peak dissipation due to bottom friction is no longer in the middle of the channel. This is because the overlapping continental barriers force the circumpolar current to either side of the center of the channel for much of its path (cf. the path of the current in Figures 4b and 4c). This can be seen as local minima in the magenta lines of Figures 6e and 6f at around $\pm$300 km.

In the case of experiment ROVER's momentum balance in Figure 6f, there is a north-south split, as in the SOLOB budget of Figure 6c. Three distinct regions can be seen:

1. North of the region where the barriers overlap, continental form stress is the largest term and acts to offset all the other terms;
2. Within the region where the barriers overlap, bottom form stress and continental form stress are of similar magnitude and both are westward;
3. South of the region where the barriers overlap, continental form stress is small, and the dominant balance is between bottom form stress and surface wind stress.

The meridional asymmetry of the integrated momentum budget can be explained by appealing to the stratification of the domain and the path of the current. Due to the steeply sloping isopycnals, which deepen to the north, the baroclinic currents tend to be stronger in the northern half of the domain in all of the model simulations. Examination of Figure 4c also indicates that, in the time mean, the current spends a larger fraction of its path to the north of the center of the channel rather than to the south. Both of these factors will contribute to a stronger push against the northern continental barrier, which allows for an increased continental form stress in this part of the domain.

The change in character of the momentum balance with the addition of overlapping continental barriers can be linked to the change in sensitivity of T_{ACC} by also meridionally integrating equation (8), such that the budget is now volume integrated. This reduces each curve in Figure 6 to a single point that summarizes the total momentum source/sink. This volume integrated momentum budget is drawn in Figures 7a and 7b for the experiments with RIDGE and ROVER geometry, with the total momentum input at the control wind stress ($\tau_0 = 0.2$ N m^{-2}) used to normalize all of the data points. Hence, the total momentum input from the wind (blue lines) varies between 0 and 2, with the experiments in Figure 6 being the set of points at 1 on the x axis.

In Figure 7a a change in total momentum input from the wind causes a concomitant change in bottom form stress. The total momentum sink due to bottom friction is very low, since the barotropic gyres of the mean flow (Figure 4b) have zero net eastward flow. As a result, the slightly nonzero bottom friction in Figure 7a reflects the very low T_b in Figure 5b. As the wind increases/decreases, the domain average EKE increases/decreases in quasi-linear proportion, as per Figure 9 of [*Munday et al.*, 2013]. This is a reflection of the dominant mechanical energy balance of circumpolar currents, in which the wind work on the surface

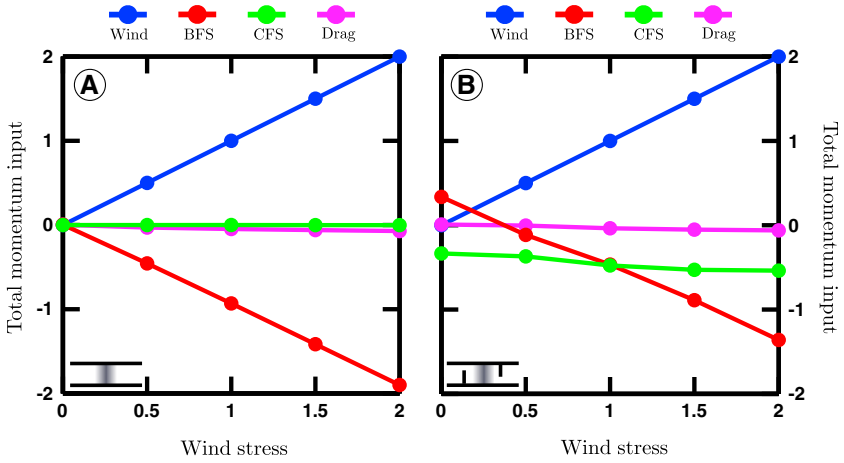

Figure 7. (a) Sensitivity to wind stress of the volume integrated momentum budget for RIDGE geometry experiments. (b) As Figure 7a for ROVER geometry. The colors match the curves in Figure 6 and indicate the corresponding term in the momentum budget, i.e., wind stress (blue), bottom form stress (red), continental form stress (green), and bottom drag (magenta). The small glyphs schematically indicate the geometry under consideration in each panel. The values have been scaled by the momentum input of the wind stress for the respective control states. Hence, there are no units.

flow is balanced by dissipation of bottom EKE [*Cessi et al.*, 2006; *Cessi*, 2008; *Abernathey et al.*, 2011], i.e.,

$$\frac{\langle \tau_s \bar{u}_s \rangle}{\rho_0} \approx r_b \frac{1}{2} \left\langle \overline{\mathbf{u}_b' \cdot \mathbf{u}_b'} \right\rangle, \tag{11}$$

where u_s is the zonal velocity at the surface. This balance is between bottom EKE and surface wind work; hence, between wind stress and (domain average) EKE, it is only quasi-linear. For those experiments with significantly nonzero bottom flow, i.e., those with a flat bottom, this balance must be modified to include the mean kinetic energy of the flow, $\frac{1}{2}\langle \bar{\mathbf{u}}_b \cdot \bar{\mathbf{u}}_b \rangle$, which may also be large.

In the presence of a bathymetric ridge, this increase in EKE allows for an increase in the eddy form stress between density layers. The result is that the bottom form stress is always able to match the momentum input from the surface wind stress, with EKE and eddy form stress changing just enough to maintain the dominant balance of Figure 6b. Since this balance is enforced by changes in the eddy field, the mean flow need not alter in response to surface wind stress changes. The result is no sensitivity of T_{ACC} to wind stress, since the eddy form stress, and thus the bottom form stress, is independent of the mean flow.

In Figure 7b, the total momentum sink due to bottom friction for the experiments with ROVER geometry again remains low for all values of τ_0. At the control wind stress, $\tau_0 = 0.2$ N m^{-2}, the bottom form stress and continental form stress are equal in magnitude and each acts as a sink for about half of the momentum input by the wind. For increases in τ_0 above the control value, the increased momentum input is offset by a stronger bottom form stress, since EKE increases and thus so can the eddy form stress between isopycnal layers. However, for lower wind stresses, the EKE and eddy form stress must decrease. As a result, the continental form stress begins to play a larger role in acting as a sink for the momentum input from the wind. Since the continental form stress depends on the mean current pushing against the continent, and the continent pushing back, it depends on the mean T_{ACC}. Hence, for $\tau_0 < 0.2$ N m^{-2}, T_{ACC} must exhibit sensitivity to the wind, as we see in Figure 5d. Much of this sensitivity arises from changes in the T_b contribution to T_{ACC}, since the push from the continent will be broadly depth-independent in nature. In some sense, then, the experiments with ROVER geometry remain eddy saturated, since the transport due to thermal wind is roughly invariant to changes in wind stress.

All of the experiments with a flat bottom exhibit sensitivity to wind forcing, see Figure 5c. Each of these experiments has the momentum input by the wind balanced by some combination of bottom friction or by the Bernoulli potential drop across one or more continental barriers. Both of these sinks of momentum are mean flow dependent, since one arises from the frictional dissipation of the mean bottom flow and the other from the rigid barrier barotropically pushing back against the total circumpolar transport. Hence, modification of the surface wind stress must be accompanied by a change in the mean flow, and T_{ACC}, in order to provide a sufficiently large sink of eastward momentum.

In the experiments without wind stress, there is no source of momentum from the external forcing. As such, if one or other of the remaining terms is nonzero, for example, if there is a continental barrier, then one of the others must change sign to balance it. This can be seen in the zero wind case with ROVER geometry (Figure 5d) as the bottom form stress becoming positive. This must be the case since thermal wind, and the direction the isopycnals slope in, produces an eastward flow. The continent then pushes back westward, and the loss of momentum is then balanced by the ridge pushing eastward. In the case of the flat-bottomed experiments, a similar result is achieved via a change in sign of the bottom friction term. This can occur because the roughly barotropic push of the continent accelerates the flow westward roughly equally, and so at depth, where thermal wind shear is low, the flow becomes westward allowing for eastward bottom friction. For the ROVER geometry, the transition to a net westward bottom flow takes place at a peak wind stress of roughly 0.025 N m^{-2}.

5. Summary and Discussion

The time frame over which Drake Passage opened between Cape Horn and the Antarctic continent is poorly constrained [*Barker and Thomas*, 2004]. In contrast, the opening of the Tasman Seaway is relatively well dated to between 35.5 Ma and 30 Ma [*Barker et al.*, 2007]. In the past, the literature has assumed that a belt of open circumpolar latitudes is a prerequisite for the formation of a circumpolar current. However, recent theoretical advances regarding the path and transport of the ACC have shown that it can migrate a considerable distance north of any open circumpolar latitude band in order to follow the wind forcing [*Allison et al.*, 2010]. This suggests that in the dim and distant past, it may have been possible for a considerable circumpolar current to have formed prior to the opening of the Tasman Seaway if Drake Passage was already open.

Experiments with an eddy-resolving model have demonstrated that it is not necessary for unblocked latitude circles, as in Drake Passage of the modern world, to exist in order to have a significant circumpolar transport. Only a traceable circumpolar path around continental barriers, such that the current can meander around the intervening obstacles, need exist to allow for a transport in excess of 50 Sv. This transport is linked to ocean stratification, a key component of ocean circulation, via thermal wind balance and so its changes and sensitivity to wind stress are of great importance.

In the case of a flat bottom, the circumpolar transport always exhibits linear sensitivity to changes in wind stress. Although the strength of this sensitivity, the gradient of the lines in Figure 5c, is sensitive to the introduction of one or more continental barriers. The addition of a bathymetric ridge, high enough to block all f/H contours and so reduce the bottom flow to almost zero, with no continents can alter the dynamics and allow for an eddy-saturated regime. In this regime there is little or no sensitivity of circumpolar transport to changes in wind stress. The introduction of continental barriers causes sensitivity to reoccur at low wind stresses, with the change being most pronounced for the case of overlapping barriers. This suggests that a young ACC may well have exhibited a different sensitivity to wind stress than its modern counterpart. However, this increased sensitivity would have most likely come about due to changes in the depth-independent part of its transport. As a result, the implications for the depth of the global pycnocline and the young ACC's baroclinic transport may be limited, although the presence of overlapping continents does lead to a distinct shallowing of the pycnocline.

Changes in sensitivity between sets of experiments can be traced to the momentum budget of the different configurations. Those experiments that exhibit sensitivity to changes in wind stress, whether for all wind stresses used or merely a subset, have the source of momentum from the wind offset by a mean flow-dependent sink. In the case of the flat-bottomed experiments, this is either bottom friction or continental form stress. When a bathymetric ridge is present, the net effect of bottom friction is low. As such, it is when these experiments rely upon changes to continental form stress to balance the injection of momentum at the surface that sensitivity to changes in wind stress emerges. In the case of the ROVER experiments, the increased sensitivity comes from changes to the depth-independent part of the flow, consistent with the continental barriers pushing against the baroclinic flow in a depth-independent manner. In a sense, these experiments are still predominantly eddy saturated, since the thermal wind flow arising from steeply sloping isopycnals is relatively invariant to wind stress.

Questions remain regarding how deep and/or wide an ocean gateway is required for the development of significant circumpolar flow. During the opening of an ocean gateway, the depth of the seabed would

deepen at the same time as the gateway widens. Our experiments do not seek to address how wide or deep Drake Passage and/or the Tasman Seaway would have to be to allow a strong circumpolar transport. An idealized model, similar to that used here, could be profitably used to independently vary both parameters (the depth and width) of the gateway and pinpoint when the transition from strong to weak circumpolar transport takes place. Without further evidence, it is difficult to speculate as to the minimum depth/width required for strong transport. One might base an estimate on the knowledge of the modern ACC and its stratification, i.e., the fronts that instantaneously carry the transport of the ACC are very narrow (<100 km), but the stratification extends down to ~1500 m. Significant bathymetry remote to a narrow constriction is less of a concern for drastic reduction of circumpolar transport, since the circumpolar current would be able to meander around shallow regions of ocean as the modern ACC does with Kerguelan Plateau.

Here we chose to separate the continental barriers in space from the bathymetric ridge, in order to facilitate the decomposition of the pressure gradient term of the momentum budget. In practice, these obstructions to the flow would have been collocated, and their respective widths and depths may have interacted with regard to obstructing the flow. Bathymetry of realistic complexity would also require multiple, irregularly shaped ridges and perhaps further constrictions to the flow. We would not expect the presence of multiple bathymetric ridges to alter the momentum balance of the current, since the high-resolution models cited in section 1 are the best evidence for the modern balance between surface wind stress and bottom form stress. The blocking of f/H contours is key to preventing strong bottom flow and allowing the modern zonal momentum balance of surface wind stress balanced by bottom form stress to emerge. However, Drake Passage and/or the Tasman Seaway would have evolved from an initially shallow state, and so it would seem very likely that in the distant past the f/H contours at one or other of these narrow constrictions would remain blocked. As a result, the modern momentum balance would likely apply even for very early circumpolar flow.

Reconstructions of paleogeography indicate a much greater continental overlap than the 500 km used in the ROVER and OVERL experiments, as per the schematic of Figure 2. Using a bigger, more realistic, overlap extent would require a bigger domain in the meridional direction, and a concomitant increase in computational expense. This would play against the strength of idealized simulations, i.e., the ability to run many experiments in a carefully chosen model domain. However, a more extreme overlap would probably accentuate the role of continental form stress in the zonal momentum budget and thus allow it to play a stronger role in the sensitivity of circumpolar transport to wind stress. This may have the result of delaying the loss of sensitivity to higher wind stresses than seen here. The change in dynamics and zonal momentum budget from our experiments would thus be more likely with a more realistic geometry, rather than less likely.

The introduction of a continental barrier removes the constraint that the surface Ekman transport must be balanced by a return flow below the shallowest topography. This may have implications for the form of the residual overturning circulation in the paleocean and its sensitivity to wind forcing, i.e., eddy compensation may be more or less applicable in the past. Similarly, this has implications for changing meridional heat transport, which is essentially the temperature-weighted meridional overturning. *Huber and Nof* [2006] find little or no evidence for changing Eocene heat transport in a synthesis of available coupled climate model results. In examining the role that an obstructed Southern Ocean might play in a simple reduced gravity model they find that increasing the length of the attached Australia can reduce the simulated meridional overturning. Changes in surface temperature and salinity forcing, which we have not addressed, would also play a role in setting the meridional overturning circulation and its sensitivity.

In a more complex model that resolves eddies and includes thermodynamics, there is an increased chance that such overturning changes could impact the heat transport. In particular, a circumpolar current that passes to the north of an attached Australia, as per Figure 2c, may be able to carry more heat southward into the Southern Ocean. Even discounting the role of a resolved eddy field, higher resolution may facilitate the current taking this northern path as shown in *Sijp et al.* [2011]. The heat transport also needs to be considered in the context of changing stratification. As a result, even if the heat transport does not alter, its partitioning, via Reynolds averaging, into mean, standing, and transient eddies may still change.

In the experiments that include overlapping barriers and a bathymetric ridge (ROVER geometry), the sensitivity of the circumpolar transport to wind stress changes resides in T_b. In a sense, these experiments are still eddy saturated, since the depth of the pycnocline and the component of the flow due to thermal wind shear are comparatively invariant. In comparing these experiments with the RIDGE geometry, there is

a clear role for the opening of the Tasman Seaway; the pycnocline deepens even as the eddy field increases in strength (as measured by the domain average EKE; see Table 2). This indicates a key role for the mesoscale eddy field in setting the stratification of the ocean both before and after the opening of this ocean gateway. Such a deepening of the stratification implies changes in eddy heat transport, perhaps due to the elimination of standing meanders, the presence of which increases the efficiency of cross-current heat transport [*Abernathey and Cessi*, 2014] and accompanying shifts in the meridional overturning toward the modern picture of deep upwelling within the confines of the Southern Ocean. In this light, proxy measurements of ACC path and strength such as sortable silt [e.g., *Pfuhl and McCave*, 2005; *McCave et al.*, 2014] may also be a useful indicator of not only when the ACC was first established as a strong, circumpolar flow but also when ocean wide changes in stratification and the establishment of deep upwelling began to occur.

Appendix A: Numerical Details

We use the vector-invariant form of the momentum equations; see equation (6). The Jamart "wet point" method [*Jamart and Ozer*, 1986] is applied to the Coriolis terms. In order to reduce numerical diapycnal diffusivity [*Griffies et al.*, 2000; *Hill et al.*, 2012], potential temperature is advected using the seventh-order advection scheme of *Daru and Tenaud* [2004]. Guided by *Griffies and Hallberg* [2000] and *Fox-Kemper and Menemenlis* [2008], lateral viscous dissipation of momentum is carried out using a modified *Leith* [1996] scheme in both harmonic (∇^2) and biharmonic (∇^4) forms. This helps prevent the viscous closure from being a further source of spurious diapycnal mixing [*Ilicak et al.*, 2012]. The side and bottom boundary conditions are no slip, and additional bottom friction is included to ensure that experiments with no bathymetry reach a stable equilibrium. Biharmonic diffusion is applied to temperature. Although this is not strictly necessary, due to the choice of advection scheme, it prevents eddies from cascading to very small scales unresolved by the grid.

Vertical viscous and diffusive processes are integrated in time implicitly and remain purely harmonic with constant coefficients. Convective adjustment is carried out by increasing the vertical diffusivity to 10 $m^2\ s^{-1}$ when static instability is present. The model uses a linear equation of state with a constant expansion coefficient for temperature and no dependence upon salinity. Relevant model parameters for all coefficients are as given in Table 1.

Acknowledgments
The model data used in this paper are available from the corresponding author upon request. This study is funded by the UK Natural Environment Research Council grant NE/H005668/1 and NE/K010948/1. D.R.M. acknowledges helpful and imaginative discussions with Xiaoming Zhai, James Maddison, Andy Hogg, Adele Morrison, Nathan Bindoff, and Maria Rugenstein. Renske Gelderloos and Helen Pillar provided useful comments on an earlier draft. D.P.M. acknowledges additional support from the Oxford Martin School. H.L.J. is supported by a Royal Society University Research Fellowship. This work made use of the facilities of HECToR, the UK's national high-performance computing service, which is provided by UoE HPCx Ltd at the University of Edinburgh, Cray Inc, and NAG Ltd, and funded by the Office of Science and Technology through EPSRCs High End Computing Programme. The authors thank the anonymous reviewers and Editors for their support of the paper and valuable criticism of the original submission that has improved the final version.

References

Abernathey, R., and P. Cessi (2014), Topographic enhancement of eddy efficiency in baroclinic equilibration., *J. Phys. Oceanogr.*, *44*, 2107–2126, doi:10.1175/JPO-D-14-0014.1.

Abernathey, R., J. Marshall, and D. Ferreira (2011), The dependence of Southern Ocean meridional overturning on wind stress, *J. Phys. Oceanogr.*, *41*, 2261–2278.

Allison, L. C., H. L. Johnson, D. P. Marshall, and D. R. Munday (2010), Where do winds drive the Antarctic Circumpolar Current?, *Geophys. Res. Lett.*, *37*, L12605, doi:10.1029/2010GL043355.

Barker, P. F., and E. Thomas (2004), Origin, signature and palaeoclimatic influence of the Antarctic Circumpolar Current, *Earth Sci. Rev.*, *66*, 143–162.

Barker, P. F., B. Diekmann, and C. Escutia (2007), Onset of Cenozoic Antarctic glaciation, *Deep Sea Res.*, *54*, 2293–2307.

Blakey, R. (2008), Gondwana paleogeography from assembly to breakup—A 500 m. y. odyssey, in *Resolving the Late Paleozoic Ice Age in Time and Space*, edited by C. R. Fielding, T. D. Frank, and J. L. Isbell, *Geol. Soc. of Am. Spec. Pap.*, *441*, 1–28.

Böning, C. W., A. Dispert, M. Visbeck, S. R. Rintoul, and F. U. Schwarzkopf (2008), The response of the Antarctic Circumpolar Current to recent climate change, *Nat. Geosci.*, *1*, 864–869.

Bryan, K., and M. D. Cox (1972), An approximate equation of state for numerical models of ocean circulation, *J. Phys. Oceanogr.*, *2*, 510–517.

Bryden, H. L. (1979), Poleward heat-flux and conversion of available potential-energy in Drake Passage, *J. Mar. Res.*, *37*, 1–22.

Cessi, P. (2008), An energy-constrained parameterization of eddy buoyancy flux, *J. Phys. Oceanogr.*, *38*, 1807–1820.

Cessi, P., W. R. Young, and J. A. Polton (2006), Control of large-scale heat transport by small-scale mixing, *J. Phys. Oceanogr.*, *36*, 1877–1894.

Danabasoglu, G., J. C. McWilliams, and P. R. Gent (1994), The role of mesoscale tracer transports in the global ocean circulation, *Science*, *264*, 1123–1126.

Daru, V., and C. Tenaud (2004), High order one-step monotonicity-preserving schemes for unsteady compressible flow calculations, *J. Comput. Phys.*, *193*, 563–594.

Fox-Kemper, B., and D. Menemenlis (2008), Can large eddy simulation techniques improve mesoscale rich ocean models?, in *Ocean Circulation and Climate, Geophys. Monogr. Ser.*, vol. 177, edited by M. W. Hecht and and H. Hasumi, pp. 319–337, AGU, Washington, D. C.

Gill, A. E., and K. Bryan (1971), Effects of geometry on the circulation of a three-dimensional Southern-Hemisphere ocean model, *Deep Sea Res.*, *18*, 685–721.

Gille, S. T. (1997), The Southern Ocean momentum balance: Evidence for topographic effects from numerical model output and altimeter data, *J. Phys. Oceanogr.*, *27*, 2219–2231.

Gnanadesikan, A. (1999), A simple predictive model for the structure of the oceanic pycnocline, *Science*, *283*, 2077–2079.
Gnanadesikan, A., and R. W. Hallberg (2000), On the relationship of the Circumpolar Current to Southern Hemisphere winds in coarse-resolution ocean models, *J. Phys. Oceanogr.*, *30*, 2013–2034.
Griffies, S. M., and R. W. Hallberg (2000), Biharmonic friction with a Smagorinsky-like viscosity for use in large-scale eddy-permitting ocean models, *Mon. Weather Rev.*, *128*, 2935–2946.
Griffies, S. M., R. C. Pacanowski, and R. W. Hallberg (2000), Spurious diapycnal mixing associated with advection in a *z*-coordinates ocean model, *Mon. Weather Rev.*, *128*, 538–564.
Hallberg, R., and A. Gnanadesikan (2001), An exploration of the role of transient eddies in determining the transport of a zonally reentrant current, *J. Phys. Oceanogr.*, *31*, 3312–3330.
Hidaka, K., and M. Tsuchiya (1953), On the Antarctic Circumpolar Current, *J. Mar. Res.*, *12*, 214–222.
Hill, C., D. Ferreira, J. M. Campin, J. Marshall, R. Abernathey, and N. Barrier (2012), Controlling spurious diapycnal mixing in eddy-resolving height-coordinate ocean models—Insights from virtual deliberate tracer release experiments, *Ocean Modell.*, *45-46*, 14–26, doi:10.1016/j.ocemod.2011.12.001.
Hill, D. J., A. M. Haywood, P. J. Valdes, J. E. Francis, D. J. Lunt, B. S. Wade, and V. C. Bowman (2013), Paleogeographic controls on the onset of the Antarctic Circumpolar Current, *Geophys. Res. Lett.*, *40*, 5199–5204, doi:10.1002/grl.50941.
Hogg, A. M. (2010), An Antarctic Circumpolar Current driven by surface buoyancy forcing, *Geophys. Res. Lett.*, *37*, L23601, doi:10.1029/2010GL044777.
Hogg, A. M., and D. R. Munday (2014), Does the sensitivity of Southern Ocean circulation depend upon bathymetric details?, *Philos. Trans. R. Soc. London, Ser. A*, *372*, 20,130,050, doi:10.1098/rsta.2013.0050.
Huber, M., and D. Nof (2006), The ocean circulation in the Southern Hemisphere and its climatic impacts in the Eocene, *Palaeogeogr. Palaeoclimatol. Palaeoecol.*, *231*, 9–28.
Huber, M., H. Brinkhuis, C. E. Stickley, K. Döös, A. Sluijs, J. Warnaar, S. A. Schellenberg, and G. L. Williams (2004), Eocene circulation of the Southern Ocean: Was Antarctica kept warm by subtropical waters?, *Paleoceanography*, *19*, PA4026, doi:10.1029/2004PA001014.
Ilicak, M., A. J. Adcroft, S. M. Griffies, and R. W. Hallberg (2012), Spurious dianeutral mixing and the role of momentum closure, *Ocean Modell.*, *45-46*, 37–58, doi:10.1016/j.ocemod.2011.10.003.
Jackson, L., C. W. Hughes, and R. G. Williams (2006), Topographic control of basin and channel flows: The role of bottom pressure torques and friction, *J. Phys. Oceanogr.*, *36*, 1786–1805.
Jamart, B. M., and J. Ozer (1986), Numerical boundary layers and spurious residual flows, *J. Geophys. Res.*, *91*, 10,621–10,631.
Jayne, S. R., and J. Marotzke (2002), The oceanic eddy heat transport, *J. Phys. Oceanogr.*, *32*, 3328–3345.
Johnson, G. C., and H. L. Bryden (1989), On the size of the Antarctic Circumpolar Current, *Deep Sea Res.*, *36*, 39–53.
Krupitsky, A., V. M. Kamenkovich, N. Naik, and M. A. Cane (1996), A linear equivalent barotropic model of the Antarctic Circumpolar Current with realistic coastlines and bottom topography, *J. Phys. Oceanogr.*, *26*, 1803–1824.
LaCasce, J. H., and P. E. Isachsen (2010), The linear models of the ACC, *Prog. Oceanogr.*, *84*, 139–157.
Leith, C. E. (1996), Stochastic models of chaotic systems, *Physica D*, *98*, 481–491.
Livermore, R., A. Nankivell, G. Eagles, and P. Morris (2005), Paleogene opening of Drake Passage, *Earth Planet. Sci. Lett.*, *236*, 459–470.
Marshall, D. (1995), Topographic steering of the Antarctic Circumpolar Current, *J. Phys. Oceanogr.*, *25*, 1636–1650.
Marshall, D. (1997), Subduction of water masses in an eddying ocean, *J. Mar. Res.*, *55*, 201–222.
Marshall, J., and T. Radko (2003), Residual-mean solutions for the Antarctic Circumpolar Current and its associated overturning circulation, *J. Phys. Oceanogr.*, *33*, 2341–2354.
Marshall, J., A. Adcroft, C. Hill, L. Perelman, and C. Heisey (1997a), A finite volume, incompressible Navier-Stokes model for studies of the ocean on parallel computers, *J. Geophys. Res.*, *102*, 5753–5766.
Marshall, J., C. Hill, L. Perelman, and A. Adcroft (1997b), Hydrostatic, quasi-hydrostatic, and non-hydrostatic ocean modeling, *J. Geophys. Res.*, *102*, 5733–5752.
Mazloff, M. R., P. Heimbach, and C. Wunsch (2010), An eddy-permitting Southern Ocean state estimate, *J. Phys. Oceanogr.*, *40*, 880–899.
McCave, I. N., S. J. Crowhurst, G. Kuhn, C. Hillenbrand, and M. P. Meredith (2014), Minimal change in Antarctic Circumpolar Current flow speed between the last glacial and Holocene, *Nat. Geosci.*, *7*, 113–116, doi:10.1038/NGEO2037.
Meijers, A. J., N. L. Bindoff, and J. L. Roberts (2007), On the total, mean, and eddy heat and freshwater transports in the Southern Hemisphere of a $\frac{1^\circ}{8} \times \frac{1^\circ}{8}$ global ocean model, *J. Phys. Oceanogr.*, *37*, 277–295.
Meijers, A. J. S., N. L. Bindoff, and S. R. Rintoul (2011), Estimating the four-dimensional structure of the Southern Ocean using satellite altimetry, *J. Atmos. Oceanic Technol.*, *28*, 548–568, doi:10.1175/2010JTECHO790.1.
Meredith, M. P., et al. (2011), Sustained monitoring of the Southern Ocean at Drake Passage: Past achievements and future priorities, *Rev. Geophys.*, *49*, RG4005, doi:10.1029/2010RG000348.
Meredith, M. P., A. C. Naveira Garabato, A. M. Hogg, and R. Farneti (2012), Sensitivity of the overturning circulation in the Southern Ocean to decadal changes in wind forcing, *J. Clim.*, *25*, 99–110, doi:10.1175/2011JCLI4204.1.
Morrison, A. K., and A. M. Hogg (2013), On the relationship between Southern Ocean overturning and ACC transport, *J. Phys. Oceanogr.*, *43*, 140–148.
Munday, D. R., L. C. Allison, H. L. Johnson, and D. P. Marshall (2011), Remote forcing of the antarctic circumpolar current by diapycnal mixing, *Geophys. Res. Lett.*, *38*, L08609, doi:10.1029/2011GL046849.
Munday, D. R., H. L. Johnson, and D. P. Marshall (2013), Eddy saturation of equilibrated circumpolar currents, *J. Phys. Oceanogr.*, *43*, 507–532.
Munk, W. H., and E. Palmén (1951), Note on the dynamics of the Antarctic Circumpolar Current, *Tellus*, *3*, 53–55.
Olbers, D. (1998), Comments on "On the obscurantist physics of "form drag" in theorizing about the Circumpolar Current", *J. Phys. Oceanogr.*, *28*, 1647–1654.
Olbers, D., D. Borowski, C. Völker, and J. Wölff (2004), The dynamical balance, transport and circulation of the Antarctic Circumpolar Current, *Antarct. Sci.*, *16*, 439–470.
Olbers, D., K. Lettman, and R. Timmermann (2007), Six circumpolar currents—On the forcing of the Antarctic Circumpolar Current by wind and mixing, *Ocean Dyn.*, *57*, 12–31.
Olbers, D., J. Willebrand, and C. Eden (2012), *Ocean Dynamics*, chap. 16, pp. 557–624.
Pfuhl, H. A., and I. N. McCave (2005), Evidence for late Oligocene establishment of the Antarctic Circumpolar Current, *Earth Planet. Sci. Lett.*, *235*, 715–728.
Russell, J. L., R. J. Stouffer, and K. W. Dixon (2006), Intercomparison of the Southern Ocean circulations in IPCC coupled model control simulations, *J. Clim.*, *19*, 4560–4574.

Scher, H. D., and E. E. Martin (2006), Timing and climatic consequences of the opening of Drake Passage, *Science*, *312*, 428–430, doi:10.1126/science.1120044.
Sijp, W. P., M. H. England, and M. Huber (2011), Effect of the deepening of the Tasman Gateway on the global ocean, *Paleoceanography*, *26*, PA4207, doi:10.1029/2011PA002143.
Sijp, W. P., A. S. von der Heydt, H. A. Dijkstra, S. Flögel, P. M. J. Douglas, and P. K. Bijl (2014), The role of ocean gateways on cooling climate on long time scales, *Global Planet. Change*, *119*, 1–22, doi:10.1016/j.gloplacha.2014.04.004.
Stevens, D. P., and V. O. Ivchenko (1997), The zonal momentum balance in an eddy-resolving general-circulation model of the Southern Ocean, *Q. J. R. Meteorol. Soc.*, *123*, 929–951.
Straub, D. N. (1993), On the transport and angular momentum balance of channel models of the Antarctic Circumpolar Current, *J. Phys. Oceanogr.*, *23*, 776–782.
Tansley, C. E., and D. P. Marshall (2001), On the dynamics of wind-driven circumpolar currents, *J. Phys. Oceanogr.*, *31*, 3258–3273.
Thompson, A. F. (2008), The atmospheric ocean: Eddies and jets in the Antarctic Circumpolar Current, *Philos. Trans. R. Soc. London, Ser. A*, *366*, 4529–4541, doi:10.1098/rsta.2008.0196.
Vallis, G. (2006), *Atmospheric and Oceanic Fluid Dynamics*, chap. 16, pp. 667–715, Cambridge Univ. Press, New York.
Viebahn, J., and C. Eden (2010), Towards the impact of eddies on the response of the Southern Ocean to climate change, *Ocean Modell.*, *34*, 150–165.
Walin, G. (1982), On the relation between sea-surface heat flow and thermal circulation in the ocean, *Tellus*, *34*, 187–195.
Ward, M. L., and A. M. Hogg (2011), Establishment of momentum balance by form stress in a wind-driven channel, *Ocean Modell.*, *40*, 133–146.
Watson, A. J., and A. C. Naveira Garabato (2006), The role of Southern Ocean mixing and upwelling in glacial-interglacial atmospheric CO_2 change, *Tellus*, *58B*, 73–87.
Webb, D. J. (1993), A simple model of the effect of the Kerguelen Plateau on the strength of the Antarctic Circumpolar Current, *Geophys. Astrophys. Fluid Dyn.*, *70*, 57–84, doi:10.1080/03091929308203587.
Wei, W., and S. W. Wise (1992), Eocene-Oligocene calcareous nannofossil magneto biochronology of the Southern Ocean, *Newsl. Stratigr.*, *26*, 119–132.